HHS Public Access

Author manuscript

NanoImpact. Author manuscript; available in PMC 2019 July 01.

Published in final edited form as:

NanoImpact. 2018 July ; 11: 82–91. doi:10.1016/j.impact.2018.02.007.

Endothelial barrier dysfunction induced by nanoparticle exposure through actin remodeling via caveolae/raft-regulated calcium signalling

Yizhong Liu[1], **Eunsoo Yoo**[1], **Gretchen J. Mahler**[1], and **Amber L. Doiron**[1]

[1]Department of Biomedical Engineering, Binghamton University, Binghamton, USA

Abstract

The rapid development of modern nanotechnology has resulted in nanomaterial being use in nearly all applications of life, raising the potential risk of nanomaterial exposure alongside the need to design safe and effective materials. Previous work has demonstrated a specific effect of gold nanoparticles (GNPs) of approximately 20 nm on endothelial barrier function *in vitro*. To expand our understanding of this size-specific effect, titanium dioxide, silicon dioxide, and polystyrene nanoparticles (NPs) in this similar size range were studied. All tested nanoparticles were found to have minimal effects on cell viability, but exhibited a significant detrimental effect on endothelial barrier function. Nanoparticles in the size range of 20 to 30 nm were internalized by endothelial cells through caveolae/raft-mediated endocytosis, causing intracellular calcium elevation by approximately 30% at 2 hours after administration, and triggering myosin light chain kinase (MLCK)-regulated actomyosin contraction. These effects culminated in an increase in endothelial monolayer permeability across all particle types within the 20–30 nm range. This nanoparticle exposure-induced endothelial barrier dysfunction may provide valuable information for designing safer nanomaterials or potential applications of this nanoparticle exposure-induced permeability effect in biomedicine.

Graphical Abstract

Corresponding author: Amber L. Doiron, M.S., Ph.D., Assistant Professor, Department of Biomedical Engineering, Binghamton University, 2625 Biotechnology Building, 85 Murray Hill Rd, Vestal, NY 13850, USA. Tel: +1 607 777 5477. adoiron@binghamton.edu.
Yizhong Liu, Department of Biomedical Engineering, Binghamton University. yliu72@binghamton.edu
Eunsoo Yoo, Department of Biomedical Engineering, Binghamton University. eyoo4@binghamton.edu
Gretchen J. Mahler, Ph.D., Associate Professor, Department of Biomedical Engineering, Binghamton University. gmahler@binghamton.edu

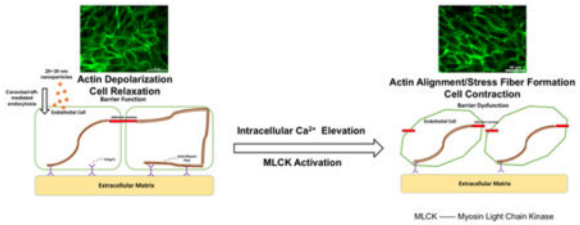

Keywords

titanium dioxide; silicon dioxide; polystyrene; gold; permeability

1. Introduction

Engineered nanoparticles (NPs), due to their controllable physiochemical properties, are heavily studied and used [1]. The increasing risk of exposure to engineered NPs has raised extensive concern over their effects on human health [2]–[5]. The endothelium at the inner lining of blood vessel walls serves as an important interface between circulating blood and surrounding tissues. The nature of the endothelium makes it a barrier that regulates the substance exchange between blood and the tissues that rely on the blood supply, supporting the entire biological system. When NPs enter the human body, accidentally or intentionally, blood circulation is the main route for their spread throughout the body. The endothelium is a critical barrier to interact with the nanoparticles, which makes endothelial barrier integrity a critical consideration when assessing the safety of nanoparticles [6]. Even though much research has been done on the impact of nanoparticle exposure on endothelial barrier function [7]–[9], there still exists widespread uncertainty about the impact of nanomaterials due to the complexity of barrier function regulation and the physicochemical property-dependent interaction between nanoparticles and cells.

Previous work in our lab has shown that uncoated, 20 nm gold nanoparticles (GNPs) cause endothelial barrier dysfunction without affecting cell viability by altering the cytoskeleton structure, while smaller or larger GNPs did not have the same effect [10]. Other recent research has also reported that nanoparticles in this size range are more likely to interact with cells [7], [8], [11]–[13]. Studies by *Setyawati, Magdiel I., et al.* and *Tay., et al.* reported very similar size-dependent endothelial permeability induced by gold, TiO_2, and SiO_2 NPs in the 20 nm size range [8], [14], [15]. To explore whether this size-specific effect was particle bulk material-dependent and further explore the underlying mechanism, other types of commonly used, organic and inorganic nanoparticles in the 20 nm size range were investigated here in addition to GNPs. Titanium dioxide (TiO_2), silicon dioxide (SiO_2), and polystyrene (PS) NPs are widely used in the food and food packaging industries, cosmetic products, and biomedical applications, which makes them the most commonly used in human contact situations [16]–[20]. The concentrations of particles studied were surface area-matched to concentrations of GNPs previously studied, which represent physiologically-relevant *in vivo* doses of nanoparticles[10]. TiO_2, SiO_2, and PS NPs in the 20 to 30 nm size range were studied for their impact on cell viability and endothelial barrier

function, with a focus on understanding the underlying mechanism of particle-cell interactions.

2. Materials and Methods

2.1 Cell Culture

Human umbilical vein endothelial cells (HUVEC, Lonza, Walkersville, MD) were cultured in endothelial cell growth medium 2 (EGM-2, Lonza) supplemented with the EGM-2 SingleQuot Kit Suppl. & Growth Factors (CC-4176, Lonza)—and grown under standard conditions (37°C, 5% CO_2, humidity).

2.2 Nanoparticles

All tested nanoparticles are commercially available. Titanium dioxide (TiO_2) (US3498) and silicon dioxide (SiO_2) (US3438) NPs were purchased from US Research Nanomaterials, Inc. (Houston, TX). Polystyrene (PS) NPs (FluoSpheres® Carboxylate-Modified, F8782) were purchased from ThermoFisher (Waltham, MA). For cell studies, stock nanoparticles were diluted appropriately to the testing concentrations in EGM-2 prior to use. In a recent review, the authors concluded an *in vivo* GNP dose range between 0.01 μg/g animal weight and 10 μg/g is suitable for biomedical applications without causing severe toxic reaction [21]. In a standard *in vivo* model, a 25 g mouse with a 1.5 mL blood volume, this GNPs dose range translates to between 0.167 – 167 μg/mL blood. Due to our focus on endothelial exposure, the tested concentrations of GNPs in the previous study were selected within this range to mimic reasonable physiologically relevant exposure. All tested concentrations of different nanoparticles in this study were normalized to match the concentrations of GNPs in the previous study based on the total surface area. Due to the complexity of the interactions between NPs, NPs and cells, as well as NPs with proteins in cell media, it is very difficult to quantify the amount of NPs that reached the cell surface [22, 23]; concentrations of NPs tested in this study were expressed as μg/mL (NPs per unit solution volume) or μg/cm^2 (NPs per unit cell surface area).

2.3 Nanoparticle Characterization

Scanning electron microscopy (SEM, Supra 55 VP, Zeiss, Thornwood, NY) was performed to obtain the dry particle size and morphology. The hydrodynamic size of nanoparticles was measured using nanoparticle tracking analysis (NTA, NanoSight NS300, Malvern, Westborough, MA) in both deionized (DI) water and EGM-2. Stock nanoparticles were diluted to an appropriate concentration for NTA and vortexed before measuring. Electrophoretic dynamic light scattering (DLS, Nano-ZS, Malvern) was used to measure zeta potential and hydrodynamic size of the nanoparticles. Stock nanoparticles were diluted, vortexed, and then 1 mL was transferred to a Malvern Capillary Zeta Potential cell for DLS measurements.

2.4 Cell Viability Assay

The effect of nanoparticle exposure on cell viability was quantified using Cell Counting Kit-8 (CCK-8, 96992, Sigma, St. Louis, MO). HUVEC were seeded in a collagen-coated 96-well cell culture plate (351172, Corning, Corning, NY) at 10,000 cells/cm2 and cultured

until fully confluent. Cells were exposed to TiO_2, SiO_2, and PS NPs at various concentrations for 24 hours. Nanoparticles were removed, cells were rinsed, and 100 μL of CCK-8 solution (10% CCK-8 in EGM-2) was added into each well. After 2 hours of incubation, the absorbance was measured at 450 nm using a plate reader (Synergy H1, BioTek, Winooski, VT). Cells exposed to 2% Triton™ X100 (X100, Sigma) served as the negative control and cells given fresh EGM-2 served as the positive control. The results were presented as percentage of the positive control.

2.5 Reactive Oxygen Species (ROS) Assay

The ROS level in HUVEC after nanoparticle exposure was measured using 2′,7′-Dichlorofluorescin diacetate (H2DCFDA, D6683, Sigma). HUVEC were seeded at 10,000 cells/cm^2 and cultured in a collagen-coated 96-well clear bottom black cell culture plate (3904, Corning) to confluence. Cells were exposed to TiO_2, SiO_2, and PS NPs at various concentrations for 24 hours. Nanoparticles were removed, cells were rinsed, and the absorbance of nanoparticle-treated HUVEC was measured at 495 nm and 529 nm, the wavelengths of interest for H2DCFDA detection. Next, 100 μL of 20 μM H2DCFDA solution (in phosphate buffered saline (PBS) supplemented with Ca^{2+} and Mg^{2+}) was added into each well. After 30 minutes of incubation, H2DCFDA was removed, cells were rinsed, and then the fluorescence intensity of each well was measured using a plate reader (Synergy H1, BioTek) with excitation and emission wavelengths of 495 nm and 529 nm, respectively. Data were compensated for absorbance caused by the presence of nanoparticles.

2.6 Fluorescein isothiocyanate (FITC) –Dextran Permeability Assay

HUVEC were seeded onto collagen-coated Transwell® (3413, Corning) inserts at 100,000 cells/cm2 and cultured until confluent, then exposed to TiO_2, SiO_2, and PS NPs at the concentrations that yield the same total surface area in EGM-2 for 2 hours, the apical chamber solution was replaced with 1 mg/mL 70-kD FITC-Dextran (46945, Sigma) in PBS supplemented with Ca^{2+} and Mg^{2+}, and the bottom chamber solution was replaced with PBS. The fluorescence signal intensity of the bottom chamber was then measured after 1 hour of incubation using a plate reader (Synergy H1, BioTek) with excitation and emission wavelengths of 485 nm and 530 nm, respectively.

2.7 Actin Alignment Measurement

Actin microfilament rearrangement in HUVEC exposed to nanoparticles was quantified using a method described in our previous study [24]. Succinctly, actin microfilament images were transformed to frequency domain images using a fast Fourier transform (FFT) with bandpass to exclude low intensity, high frequency noise. The waveforms of the transformed images were divided into 18 angle bands; spanning from 0 to 180 degrees for easier distribution analysis. Total pixel intensities of each angle band were calculated, and then the coefficient of variation of the intensity distribution among all 18 angle bands was calculated. The coefficient of variation was then converted into an alignment index for easier interpretation [25]. An index of 0 corresponds to an even distribution over all angle bands (no alignment), while an index of 1 corresponds to a total distribution in one angle band (complete alignment). Samples were analysed after 2 hours of exposure. All samples were imaged on an inverted wide field fluorescence microscope (Eclipse Ti, Nikon, Melville,

NY). All image analysis was performed with NIH IMAGEJ software and MATLAB® (Mathworks, Natick, MA).

2.8 Caveolae/Raft-Dependent Endocytosis Inhibition

Various studies of the uptake of NPs by cells have shown that the internalization of NPs is size-dependent, and NPs in the 20 nm size range are primarily internalized through caveolae/raft-dependent endocytosis [26–28]. Although it is likely that several uptake mechanisms play a role in nanoparticle internalization, especially with polydisperse or aggregated particles, to investigate the caveolae/raft-dependent endocytosis of NPs the chemical inhibitor Nystatin was employed. Nystatin interferes with caveolae/raft-mediated transmembrane transportation by cholesterol sequestration and was used to decrease nanoparticle internalization through the caveolae/raft-dependent endocytosis pathway [29]. HUVEC were pre-treated with 25 μM Nystatin (N6261, Sigma) in 0.5% DMSO for 2 hours before nanoparticle exposure. HUVEC were then exposed to TiO_2, SiO_2, PS NPs, and GNPs in EGM-2 for 2 hours, fixed with 4% paraformaldehyde (PFA), and labelled for actin (Alexa Fluor® 488 Phalloidin, ThermoFischer Scientific). Samples were imaged and quantified for actin alignment. Only 20 nm PS NPs were used to demonstrate cellular uptake of nanoparticles since the fluorescence of the PS NPs made them easier to visualize.

2.9 Calcium Channel Blocker

Due to the association of the L-type calcium channels and caveolae [30], the L-type calcium channels were selectively blocked. To study the effect of nanoparticle exposure on cellular calcium homeostasis, cells were treated with 10 μM Nifedipine (N7634, Sigma), a L-type calcium channel blocker that binds to the N terminals of the calcium channels to block the inward movement of calcium, for 2 hours prior to nanoparticle exposure. HUVEC were then exposed to TiO_2, SiO_2, PS NPs, and GNPs for 2 hours, fixed with 4% PFA, and 9 nalysed for actin (Alexa Fluor® 488 Phalloidin, ThermoFisher Scientific) and nucleus (DAPI, D1306, ThermoFisher Scientific). Samples were imaged and analysed for actin rearrangement.

2.10 Intracellular Calcium Level Measurement

The intracellular Ca^{2+} level was measured after nanoparticle exposure. HUVEC were seeded and cultured to confluence in a collagen-coated 96 well flat, clear bottom black polystyrene TC-treated microplate (3904, Corning), then exposed to TiO_2, SiO_2, PS NPs, and GNPs in EGM-2 for 2 hours. Caveolae/raft-mediated endocytosis was inhibited by Nystatin and the L-type calcium channels were selectively blocked Nifedipine. After nanoparticle exposure, the cells were loaded with a high-affinity Ca^{2+} dye, Fura-2 (Fura-2 AM, ThermoFisher Scientific), by incubating the cells with 4 μM Fura-2 (diluted in PBS) for 30 minutes at room temperature in the dark, with 0.04% Pluronic® F-127 (P2443, Sigma) in the loading buffer to facilitate loading. After 30 minutes of incubation, the cells were rinsed twice with warm PBS and incubated with PBS for 15 minutes at room temperature in the dark to allow for cleavage of the AM ester, trapping the Fura-2 inside of the cells. Then the fluorescence intensity of each well was measured using a plate reader (Synergy H1, BioTek) with excitation wavelengths of 340/380 nm, and emission wavelength of 510 nm. The ratio of

fluorescence measured after excitation at the two wavelengths (F340/F380) was proportional to the intracellular free calcium concentration.

2.11 Statistical Analysis

All analyses were performed with Excel (Microsoft 2016, Redmond, WA). All data were analysed using ANOVA with Tukey's post test. All presented data are mean ± standard deviation (SD) of the sample, p values <0.05 were considered significant, and * represents significant difference from the control group.

3. Results

3.1 Nanoparticle Characterization

The morphology of all three types of nanoparticles was found to be relatively spherical when imaged using SEM (Figure 1). The dry size of all three types of nanoparticles was measured from SEM images (Table 1), and found to be relatively consistent with manufacture reported values. The zeta potential and hydrodynamic size of nanoparticles in aqueous solution (DI water and EGM-2) were acquired using NTA and DLS (Table 1), and suggested all nanoparticles were moderately stable in aqueous solution. DLS data of PS NPs was not presented because of the excitation wavelength of the dye conjugated to PS NPs overlapped with the DLS laser, which led to false readings.

3.2 Nanoparticles Exposure Did Not Cause Cell Death in HUVEC

HUVEC viability was assessed using the CCK-8 assay kit. No statistically significant change in HUVEC viability was measured after 24 hours of nanoparticle exposure at the tested concentrations (Figure 2).

3.3 Nanoparticle Exposure Induced Oxidative Stress in HUVEC

The reactive oxygen species (ROS) level in HUVEC exposed to TiO_2, SiO_2, and PS NPs at several concentrations for 24 hours was measured using H2DCFDA. The ROS level increased after nanoparticle exposure in a material- and concentration-dependent manner ($p<0.05$). Similar to previous work with other epithelial cell types, TiO_2 NPs increased the ROS level in HUVEC at almost all tested concentrations [9], while increases in SiO_2 and PS NPs-treated cells only occurred at higher concentrations (Figure 3).

3.4 Nanoparticle Exposure Disrupted Endothelial Barrier Function

The endothelial barrier function of the HUVEC monolayer exposed to TiO_2, SiO_2, and PS NPs was evaluated by measuring the permeability of FITC-Dextran. The results showed a considerable increase in HUVEC monolayer permeability after 2 hours of exposure to TiO_2, SiO_2, and PS NPs (Figure 4, $p<0.05$), indicating that exposure to TiO_2, SiO_2, and PS NPs caused endothelial barrier dysfunction at a mid-range treatment concentration.

3.5 Actin Rearrangements Induced by Nanoparticles Exposure

To investigate whether exposure to TiO_2, SiO_2, and PS NPs caused endothelial barrier dysfunction by triggering cytoskeletal structural alteration, actin alignment was measured.

HUVEC were exposed to nanoparticles for 2 hours, fixed and analyzed with ImageJ [31] and MATLAB [24] for actin alignment. Actin rearrangement compared to control was observed in HUVEC treated with TiO_2, SiO_2, and PS NPs (Figure 5) at moderate concentration, and the quantification of actin alignment (Figure 5E) ($p < 0.05$) showed a significant difference for every type of NPs compared with control, no significant difference between different type of NPs was observed. Three independent experiments of each condition were performed and 5 images were taken from each experiment; a total 15 images of each condition were analysed.

3.6 The Internalization of Polystyrene Nanoparticles via the Caveolae/Raft-Dependent Endocytosis Pathway

The PS NPs in this study are fluorescent, allowing straightforward visualization using fluorescence microscopy. Confluent HUVEC monolayers exposed to 20 nm PS NPs at 2.18 μg/mL for 2 hours were fixed, stained for actin and nucleus, and imaged for actin (green), nucleus (blue), and PS NPs (red). Actin alignment and stress fiber formation was observed (Figure 6G), and the overlapped image of the nucleus and PS NPs (Figure 6H) exhibited a nuclei-surrounding distribution of PS NPs, suggesting the internalization of PS NPs into the cytosol. The caveolae/raft-mediated endocytosis inhibitor, Nystatin was used to inhibit internalization via the caveolae/raft-dependent endocytosis pathway. HUVEC pretreated with Nystatin did not show actin alignment, and the presence of PS NPs was significantly reduced (Figure 6E, F). Quantification of actin alignment also showed the inhibition of caveolae/raft-dependent endocytosis by Nystatin successfully prevented actin rearrangement/alignment after PS nanoparticle exposure (Figure 6I) ($p < 0.05$).

3.7 Intracellular Calcium Level Elevation Caused by Nanoparticles Exposure

HUVEC were pretreated with caveolae/raft-mediated endocytosis inhibitor Nystatin or the L-type calcium channels blocker Nifedipine prior to nanoparticle exposure, and the intracellular Ca^{2+} level was measured using Fura-2 AM. In HUVEC exposed to TiO_2, SiO_2, PS NPs, and GNPs for 2 hours, the intracellular Ca^{2+} level increased over 30% compared to untreated HUVEC. Either blocking the L-type calcium channel or inhibiting the caveolae/raft-mediated endocytosis significantly reduced the nanoparticle exposure-induced intracellular Ca^{2+} elevation (Figure 7).

3.8 Intracellular Calcium Level Elevation Triggered Actin Rearrangement

Given the involvement of intracellular calcium in the regulation of myosin light chain kinase (MLCK), and the intracellular calcium elevation induced by nanoparticle exposure, we hypothesized that the nanoparticle exposure-induced actin rearrangement was caused by intracellular calcium elevation. To test the hypothesis, HUVEC were pretreated with caveolae/raft-mediated endocytosis inhibitor Nystatin or the L-type calcium channels blocker Nifedipine prior to nanoparticle exposure. HUVEC pretreated with Nystatin or Nifedipine did not show actin alignment after nanoparticle exposure, while actin rearrangement/alignment was observed in HUVEC that are not pretreated with Nystatin or Nifedipine compared to control. Quantification of actin alignment (Figure 8) showed that blocking the L-type calcium channels or inhibiting caveolae/raft-mediated endocytosis prevented actin rearrangement.

4. Discussion

It is well known that the effects of nanoparticle exposure on cell viability and cellular function are size, concentration, and surface modification-dependent, but the complexity of the impact of particle physicochemical properties on biological systems remains poorly understood. We evaluated a library of GNPs in different sizes and with or without PEG surface modification in our previous study, finding all tested GNPs did not induce significant cell viability loss, but only 20 nm GNPs without PEG coating can cause endothelial barrier dysfunction by triggering actin microfilaments rearrangement [10]. In this study, three types of commonly used nanoparticles, TiO_2 NPs, SiO_2 NPs, and PS NPs, in a 20–30 nm size range were selected to further investigate this size-specific effect of GNPs on endothelial barrier function. TiO_2 NPs, SiO_2 NPs, and PS NPs, in 20 nm size range were found to have minimal effect on HUVEC viability at all tested concentrations at 24 hours of exposure time. Even though no significant effect on cell viability was observed in this study, we show that all three types of particles in 20 nm size range can affect cellular morphology and barrier function, measured as a change in cell monolayer permeability. These findings are consistent with the previous findings in GNPs [24].

It is well established that endothelial cell monolayer permeability is directly regulated by actomyosin contraction [32], [33]. In the endothelial monolayer, actin microfilaments form a cortical bundle that is involved in both cell-cell connections and cell-ECM adhesion and also support the cellular skeletal structure [34]. This involvement of actin in regulating the cytoskeleton plays a very important role in the maintenance of the barrier function of the endothelium [35]. During polarization of the cytoskeleton, the phosphorylation of actin, which is regulated by MLCK, promotes the formation of stress fibers, causing actomyosin contraction and resulting in barrier dysfunction. By contrast, during the depolarization of the cytoskeleton, the dephosphorylation of actin as regulated by myosin light chain phosphatase (MLCP) facilitates the reduction of stress fibers, causes actomyosin relaxation, and results in barrier function enhancement [36]. In the studies by *Setyawati, Magdiel I., et al.*, the authors reported the cell-cell junction gap formation after nanoparticle exposure and the link between endothelial leakiness and junction gap formation. The results in this present study showed actin microfilament rearrangement and stress fiber formation in HUVEC after exposure to TiO_2, SiO_2, PS NPs, and GNPs in the roughly 20 nm size range. The quantification of the directionality of the actin microfilaments supported our observation, indicating this size-specific nanoparticle exposure-induced actin microfilament rearrangement and stress fiber formation may be partially responsible for the endothelial barrier dysfunction [8], [11], [14], [15]. In our previous work with GNPs, endothelial permeability disruption was recorded as early as one hour after GNPs administration, which is in agreement with the study on TiO_2 NPs by *Setyawati, Magdiel I., et al.* [8]. However, no quantifiable actin microfilament directionality change was observed until 2 hours after GNPs administration, also suggesting this actin microfilament rearrangement and stress fiber formation may be only one part of the mechanism of nanoparticle exposure-induced endothelium leakage.

Size is one of the most important physical properties of nanoparticles; it contributes directly to the fate of nanoparticles in a biological system [37], [38]. Images of HUVEC exposed to

20 nm PS NPs suggested a possible localization of particles near the nucleus within the cytosol in HUVEC. Numerous researchers have shown the uptake or internalization of nanoparticles by cells is size-dependent [26], [39]. Recent studies have reported the uptake of nanoparticles is inversely proportional to the size of nanoparticles; as the size of nanoparticles increases, the internalization of nanoparticles by cells dramatically decreases [40], [41]. Interestingly, studies have shown a much higher uptake of nanoparticles in the roughly 20 nm size range by cells than other sizes [28], [42], and an analytical model derived from experimental data created by *Sulin Zhang et al.,* suggests the peak uptake of nanoparticles occurs to nanoparticles between 20 to 30 nm [43]. This size range is highly consistent with the size range of nanoparticles that caused endothelial barrier dysfunction in this study. Even the size characterization of the studied NPs suggested aggregations of NPs in aqueous solution, the size distribution still showed considerable numbers of particles within 20 to 30 nm size range, implying the internalization of nanoparticles might be the starting point of this nanoparticle-induced barrier dysfunction in endothelial monolayers.

The internalization of nanoparticles by cells is size-dependent, and different endocytosis pathways are involved in the intake of particles of different size ranges. Since the size of nanoparticles of interest here is 20 to 30 nm, the internalization of nanoparticles was most likely through the caveolae/raft-mediated endocytosis pathway [44]. To verify this hypothesis, a caveolae/raft-mediated endocytosis specific inhibitor, Nystatin [45], was used in HUVEC exposed to nanoparticles. HUVEC pretreated with Nystatin showed a significant reduction of nanoparticle uptake, and actin rearrangement was not observed compared with HUVEC without Nystatin treatment. This indicates the internalization of nanoparticles through the caveolae/raft-mediated endocytosis pathway was likely the starting point of the nanoparticle exposure-induced endothelial barrier dysfunction. However, the internalization of particles was not quantified in this study due to the difficulty of differentiating particles on the surface of cells compared to internalized particles. It is likely that different internalization rates into endothelial cells exist for the particle types tested due to different surface properties of the particles, and this may have affected the measured results. The completeness of the Nystatin block was also not quantified here since this study was intended to highlight the importance of caveolae/raft-mediated endocytosis as opposed to quantifying its contribution amongst other possible internalization routes for NPs by endothelial cells.

Caveolae and lipid rafts are not only involved in cytoplasmic membrane trafficking but also participate in many other important cellular regulation and signalling pathways [46], [47]. One of the most important functions of caveolae and lipid rafts is the regulation of transmembrane ion channels and ion pumps, especially the calcium ion channels [48], [49]. The importance of calcium signalling and calcium homeostasis in cell biology is well-known [50]. Once calcium ions enter the cytoplasm, they exert regulatory effects on many enzymes and proteins, and they can act directly in signal transduction or as a secondary messengers triggered by indirect signal transduction pathways [51], [52]. The entrance of calcium ions from the extracellular environment into the cytoplasm via transmembrane calcium ion channels increases the intracellular calcium level, and free calcium ions bind to a special calcium binding protein, calmodulin. The calcium-calmodulin complex activates MLCK, which leads to cell contraction [53], [54]. Caveolae abundantly exist in endothelial cells

[55], [56]. The internalization of nanoparticles via caveolae/raft-mediated endocytosis is very likely to influence caveolae/raft-related regulation and cellular signalling, particularly with respect to the calcium ion channel due to the possible activation of MLCK by calcium ion influx. The intracellular calcium level was measured after nanoparticle exposure, and results showed an approximate 30% increase after 2 hours of exposure. Alteration of the intracellular calcium level was prevented by inhibiting caveolae/raft-mediated endocytosis using Nystatin, which resulted in significantly less nanoparticle exposure-induced actin rearrangement. These findings indicate the elevation of intracellular calcium levels caused by caveolae/raft-mediated internalization of nanoparticles also contributed to nanoparticle exposure-induced endothelial barrier dysfunction. A L-type calcium channel blocker, Nifedipine, was also used to validate the effect of intracellular calcium alteration on endothelial barrier function. HUVEC pretreated with Nifedipine did not show intracellular calcium elevation and actin rearrangement after nanoparticle exposure. This further confirmed the effect of intracellular calcium alteration on endothelial barrier function.

In addition, TiO_2 NPs, SiO_2 NPs, and PS NPs exposure can induced oxidative stress, cause intracellular ROS elevation in endothelial cells. Similar results have also been found in other studies [9], [57]–[59]. Recent research has reported that increased oxidative stress can also cause cell morphology changes and increased the endothelial barrier dysfunction [2], [60], but our previous study showed reduced ROS level after gold nanoparticle exposure [10]. However, further study is needed to investigate the implications of oxidative stress in these cells, including changes in protein or gene expression. This further research would help to determine the effects of the interaction between NPs and cells and the role of oxidative stress in nanoparticle exposure-induced endothelial dysfunction. Furthermore, the endothelium is a dynamic barrier that varies greatly in barrier function and permeability with location within the body, and these studies should be repeated with different lines of human endothelial cells and in the presence of shear stress to better understand the physiological relevance of nanoparticle exposure.

Overall, based on our previous study of 20 nm GNPs, this present study examined three different types of nanoparticles in 20 nm size range and found these nanoparticles can cause barrier dysfunction in endothelial cells without significant effect on cell viability. A possible mechanism was proposed and investigated, the size-specific internalization of nanoparticles through caveolae/raft-mediated endocytosis by HUVEC caused intracellular calcium level elevation, and activated MLCK, which promoted actin rearrangement, stress fiber formation, and actomyosin contraction. The result of this cascade was endothelial barrier dysfunction.

5. Conclusions

In summary, this work demonstrated the effect of exposure to a subset of nanoparticles on endothelial barrier function. Nanoparticles in 20 nm size range can be easily internalized by endothelial cells via caveolae/raft-mediated endocytosis, which upregulates intracellular calcium, causing actomyosin contraction regulated by myosin light chain kinase, which leads to endothelial barrier dysfunction. A similar phenomenon of nanoparticle exposure-induced endothelial barrier dysfunction and morphology change has been found in other engineered nanoparticles of this size range [8], but the underlying cause was not well

explored. Findings from this work suggest that nanoparticles in 20 nm size are able to increase endothelial barrier permeability without affecting cell viability, possibly giving these particles great potential in drug delivery applications to increase cellular permeability or by altering cellular calcium homeostasis, with implications in cardiac drug and skin diseases treatment development, where calcium signalling is highly relevant. This work advances our understanding of the interplay between physiology and nanomaterials, hopefully advancing efforts towards safer nanoparticles.

Acknowledgments

Funding

Funding for this work was provided by the National Institutes of Health (1R15 ES022828).

Abbreviations

GNPs	gold nanoparticles
NPs	nanoparticles
MLCK	myosin light chain kinase
PEG	polyethylene glycol
TiO2	titanium dioxide
SiO2	silicon dioxide
PS	polystyrene
HUVEC	human umbilical vein endothelial cells
EGM-2	endothelial cell growth medium 2
SEM	scanning electron microscopy
NTA	nanoparticle tracking analysis
DI	deionized
DLS	dynamic light scattering
CCK-8	cell counting kit 8
ROS	reactive oxygen species
H2DCFDA	2′,7′-Dichlorofluorescin diacetate
PBS	phosphate buffered saline
FITC	fluorescein isothiocyanate
FFT	fast Fourier transform
MLCP	myosin light chain phosphate

References

1. Sahoo SK, Parveen S, Panda JJ. The present and future of nanotechnology in human health care. Nanomedicine Nanotechnol Biol Med. Mar; 2007 3(1):20–31.
2. Limbach LK, Wick P, Manser P, Grass RN, Bruinink A, Stark WJ. Exposure of Engineered Nanoparticles to Human Lung Epithelial Cells: Influence of Chemical Composition and Catalytic Activity on Oxidative Stress. Environ Sci Technol. Jun; 2007 41(11):4158–4163. [PubMed: 17612205]
3. Simkó M, Mattsson MO. Risks from accidental exposures to engineered nanoparticles and neurological health effects: A critical review. Part Fibre Toxicol. Dec.2010 7(1):42. [PubMed: 21176150]
4. Baun A, Hartmann NB, Grieger K, Kusk KO. Ecotoxicity of engineered nanoparticles to aquatic invertebrates: a brief review and recommendations for future toxicity testing. Ecotoxicology. Jul; 2008 17(5):387–395. [PubMed: 18425578]
5. Hassellöv M, Readman JW, Ranville JF, Tiede K. Nanoparticle analysis and characterization methodologies in environmental risk assessment of engineered nanoparticles. Ecotoxicology. Jul; 2008 17(5):344–361. [PubMed: 18483764]
6. Engin AB, Neagu M, Golokhvast K, Tsatsakis A. Nanoparticles and endothelium: An update on the toxicological interactions. Farmacia. 2015; 63(6):792–804.
7. Brun E, Carrière M, Mabondzo A. In vitro evidence of dysregulation of blood–brain barrier function after acute and repeated/long-term exposure to TiO2 nanoparticles. Biomaterials. Jan; 2012 33(3): 886–896. [PubMed: 22027597]
8. Setyawati MI, et al. Titanium dioxide nanomaterials cause endothelial cell leakiness by disrupting the homophilic interaction of VE–cadherin. Nat Commun. Apr.2013 4:1673. [PubMed: 23575677]
9. Guo Z, Martucci NJ, Moreno-Olivas F, Tako E, Mahler GJ. Titanium dioxide nanoparticle ingestion alters nutrient absorption in an in vitro model of the small intestine. NanoImpact. Jan.2017 5:70–82. [PubMed: 28944308]
10. Liu Y, et al. Nanoparticle size-specific actin rearrangement and barrier dysfunction of endothelial cells. Nanotoxicology. Aug; 2017 11(7):846–856. [PubMed: 28885066]
11. Setyawati MI, Tay CY, Leong DT. The gap between endothelial cells: key to the quick escape of nanomaterials? Nanomed. Aug; 2014 9(11):1591–1594.
12. Trickler WJ, et al. Silver Nanoparticle Induced Blood-Brain Barrier Inflammation and Increased Permeability in Primary Rat Brain Microvessel Endothelial Cells. Toxicol Sci. Nov; 2010 118(1): 160–170. [PubMed: 20713472]
13. Liu Y, Maiorana CH, Rogel N, Mahler G, German GK, Doiron AL. Towards safer nanomaterials: Investigating endothelial cell mechanical properties and barrier function. Biomedical Engineering Conference (NEBEC), 2015 41st Annual Northeast; 2015. 1–2.
14. Setyawati MI, Tay CY, Bay BH, Leong DT. Gold Nanoparticles Induced Endothelial Leakiness Depends on Particle Size and Endothelial Cell Origin. ACS Nano. May; 2017 11(5):5020–5030. [PubMed: 28422481]
15. Tay CY, Setyawati MI, Leong DT. Nanoparticle Density: A Critical Biophysical Regulator of Endothelial Permeability. ACS Nano. Mar; 2017 11(3):2764–2772. [PubMed: 28287706]
16. Weir A, Westerhoff P, Fabricius L, Hristovski K, von Goetz N. Titanium Dioxide Nanoparticles in Food and Personal Care Products. Environ Sci Technol. Feb; 2012 46(4):2242–2250. [PubMed: 22260395]
17. Gondikas AP, von der Kammer F, Reed RB, Wagner S, Ranville JF, Hofmann T. Release of TiO2 Nanoparticles from Sunscreens into Surface Waters: A One-Year Survey at the Old Danube Recreational Lake. Environ Sci Technol. May; 2014 48(10):5415–5422. [PubMed: 24689731]
18. Darvin ME, et al. Safety Assessment by Multiphoton Fluorescence/Second Harmonic Generation/ Hyper-Rayleigh Scattering Tomography of ZnO Nanoparticles Used in Cosmetic Products. Skin Pharmacol Physiol. Jun; 2012 25(4):219–226. [PubMed: 22653438]
19. Danhier F, Ansorena E, Silva JM, Coco R, Le Breton A, Préat V. PLGA-based nanoparticles: An overview of biomedical applications. J Controlled Release. Jul; 2012 161(2):505–522.

20. Han C, Romero N, Fischer S, Dookran J, Berger A, Doiron AL. Recent developments in the use of nanoparticles for treatment of biofilms. Nanotechnol Rev. 0(0):2017.
21. Khlebtsov N, Dykman L. Biodistribution and toxicity of engineered gold nanoparticles: a review of in vitro and in vivo studies. Chem Soc Rev. 2011; 40(3):1647–1671. [PubMed: 21082078]
22. Aggarwal P, Hall JB, McLeland CB, Dobrovolskaia MA, McNeil SE. Nanoparticle interaction with plasma proteins as it relates to particle biodistribution, biocompatibility and therapeutic efficacy. Adv Drug Deliv Rev. Jun; 2009 61(6):428–437. [PubMed: 19376175]
23. Nel AE, et al. Understanding biophysicochemical interactions at the nano–bio interface. Nat Mater. Jul.2009 8(7):543. [PubMed: 19525947]
24. Liu Y, et al. Nanoparticle Size-Specific Actin Rearrangement and Barrier Dysfunction of Endothelial Cells. Nanotoxicology. 2017
25. van der Meer AD, Poot AA, Feijen J, Vermes I. Analyzing shear stress-induced alignment of actin filaments in endothelial cells with a microfluidic assay. Biomicrofluidics. Mar.2010 4(1)
26. He C, Hu Y, Yin L, Tang C, Yin C. Effects of particle size and surface charge on cellular uptake and biodistribution of polymeric nanoparticles. Biomaterials. May; 2010 31(13):3657–3666. [PubMed: 20138662]
27. Panariti A, Miserocchi G, Rivolta I. The effect of nanoparticle uptake on cellular behavior: disrupting or enabling functions? Nanotechnol Sci Appl. Sep.2012 5:87–100. [PubMed: 24198499]
28. Wang Z, Tiruppathi C, Minshall RD, Malik AB. Size and Dynamics of Caveolae Studied Using Nanoparticles in Living Endothelial Cells. ACS Nano. Dec; 2009 3(12):4110–4116. [PubMed: 19919048]
29. Chen Y, Wang S, Lu X, Zhang H, Fu Y, Luo Y. Cholesterol sequestration by nystatin enhances the uptake and activity of endostatin in endothelium via regulating distinct endocytic pathways. Blood. Jun; 2011 117(23):6392–6403. [PubMed: 21482707]
30. Kamp T. Caveolae and L-type Calcium Channels in Cardiomyocytes. Grantome.
31. Schneider CA, Rasband WS, Eliceiri KW. NIH Image to ImageJ: 25 years of image analysis. Nat Methods. Jul; 2012 9(7):671–675. [PubMed: 22930834]
32. Birukova AA, et al. Endothelial permeability is controlled by spatially defined cytoskeletal mechanics: Atomic force microscopy force mapping of pulmonary endothelial monolayer. Nanomedicine Nanotechnol Biol Med. Mar; 2009 5(1):30–41.
33. Gulino-Debrac D. Mechanotransduction at the basis of endothelial barrier function. Tissue Barriers. Apr.2013 1(2)
34. Prasain N, Stevens T. The actin cytoskeleton in endothelial cell phenotypes. Microvasc Res. Jan; 2009 77(1):53–63. [PubMed: 19028505]
35. Lee JSY, Gotlieb AI. Microtubule–actin interactions may regulate endothelial integrity and repair. Cardiovasc Pathol. May; 2002 11(3):135–140. [PubMed: 12031763]
36. Shen Q, Rigor RR, Pivetti CD, Wu MH, Yuan SY. Myosin light chain kinase in microvascular endothelial barrier function. Cardiovasc Res. Jul; 2010 87(2):272–280. [PubMed: 20479130]
37. Tan J, Shah S, Thomas A, Ou-Yang HD, Liu Y. The influence of size, shape and vessel geometry on nanoparticle distribution. Microfluid Nanofluidics. Jan; 2013 14(1–2):77–87. [PubMed: 23554583]
38. Walkey CD, Olsen JB, Guo H, Emili A, Chan WCW. Nanoparticle Size and Surface Chemistry Determine Serum Protein Adsorption and Macrophage Uptake. J Am Chem Soc. Feb; 2012 134(4):2139–2147. [PubMed: 22191645]
39. Yin Win K, Feng S-S. Effects of particle size and surface coating on cellular uptake of polymeric nanoparticles for oral delivery of anticancer drugs. Biomaterials. May; 2005 26(15):2713–2722. [PubMed: 15585275]
40. Bergin IL, Witzmann FA. Nanoparticle toxicity by the gastrointestinal route: evidence and knowledge gaps. Int J Biomed Nanosci Nanotechnol. 2013; 3(1–2)
41. Doiron AL, Clark B, Rinker KD. Endothelial nanoparticle binding kinetics are matrix and size dependent. Biotechnol Bioeng. Dec; 2011 108(12):2988–2998. [PubMed: 21766288]

42. Jin H, Heller DA, Sharma R, Strano MS. Size-Dependent Cellular Uptake and Expulsion of Single-Walled Carbon Nanotubes: Single Particle Tracking and a Generic Uptake Model for Nanoparticles. ACS Nano. Jan; 2009 3(1):149–158. [PubMed: 19206261]
43. Zhang S, Li J, Lykotrafitis G, Bao G, Suresh S. Size-Dependent Endocytosis of Nanoparticles. Adv Mater Deerfield Beach Fla. 2009; 21:419–424.
44. Wang Z, Tiruppathi C, Minshall RD, Malik AB. Nanoparticle Internalization and Transport by Caveolae. FASEB J. Apr.2010 24(1 Supplement):820.1-820.1.
45. Nabi IR, Le PU. Caveolae/raft-dependent endocytosis. J Cell Biol. May; 2003 161(4):673–677. [PubMed: 12771123]
46. Simons K, Toomre D. Lipid rafts and signal transduction. Nat Rev Mol Cell Biol. Oct; 2000 1(1): 31–39. [PubMed: 11413487]
47. Brown DA, London E. Functions of Lipid Rafts in Biological Membranes. Annu Rev Cell Dev Biol. 1998; 14(1):111–136. [PubMed: 9891780]
48. Pani B, Singh BB. Lipid rafts/caveolae as microdomains of calcium signaling. Cell Calcium. Jun; 2009 45(6):625–633. [PubMed: 19324409]
49. Murata T, Lin MI, Stan RV, Bauer PM, Yu J, Sessa WC. Genetic Evidence Supporting Caveolae Microdomain Regulation of Calcium Entry in Endothelial Cells. J Biol Chem. Jun; 2007 282(22): 16631–16643. [PubMed: 17416589]
50. Carafoli E. Intracellular Calcium Homeostasis. Annu Rev Biochem. 1987; 56(1):395–433. [PubMed: 3304139]
51. Ogawa Y, Takai Y, Kawahara Y, Kimura S, Nishizuka Y. A new possible regulatory system for protein phosphorylation in human peripheral lymphocytes. I. Characterization of a calcium-activated, phospholipid-dependent protein kinase. J Immunol. Oct; 1981 127(4):1369–1374. [PubMed: 7276562]
52. Croall DE, DeMartino GN. Calcium-activated neutral protease (calpain) system: structure, function, and regulation. Physiol Rev. Jul; 1991 71(3):813–847. [PubMed: 2057527]
53. Uehata M, et al. Calcium sensitization of smooth muscle mediated by a Rho-associated protein kinase in hypertension. Nature. Oct; 1997 389(6654):990–994. [PubMed: 9353125]
54. Bremel RD. Myosin linked calcium regulation in vertebrate smooth muscle. Nature. Nov; 1974 252(5482):405–407. [PubMed: 4279340]
55. Lisanti MP, et al. Characterization of caveolin-rich membrane domains isolated from an endothelial-rich source: implications for human disease. J Cell Biol. Jul; 1994 126(1):111–126. [PubMed: 7517942]
56. Minshall RD, Sessa WC, Stan RV, Anderson RGW, Malik AB. Caveolin regulation of endothelial function. Am J Physiol - Lung Cell Mol Physiol. Dec; 2003 285(6):L1179–L1183. [PubMed: 14604847]
57. BarathManiKanth S, et al. Anti-oxidant effect of gold nanoparticles restrains hyperglycemic conditions in diabetic mice. J Nanobiotechnology. Jul.2010 8:16. [PubMed: 20630072]
58. Bhattacharjee S, et al. Role of membrane disturbance and oxidative stress in the mode of action underlying the toxicity of differently charged polystyrene nanoparticles. RSC Adv. 2014; 4(37): 19321–19330.
59. Manke A, Wang L, Rojanasakul Y. Mechanisms of Nanoparticle-Induced Oxidative Stress and Toxicity. BioMed Res Int. Aug.2013 2013:e942916.
60. Buyukhatipoglu K, Clyne AM. Superparamagnetic iron oxide nanoparticles change endothelial cell morphology and mechanics via reactive oxygen species formation. J Biomed Mater Res A. Jan; 2011 96A(1):186–195.

Research Highlights

- Nanoparticles in the 20 to 30 nm size range can cause endothelial barrier dysfunction without affecting cell proliferation.
- Nanoparticles in the 20 to 30 nm size range are primarily internalized by caveolae/raft-regulated endocytosis.
- Intracellular calcium level elevation induced by nanoparticle exposure triggers actin remodelling.

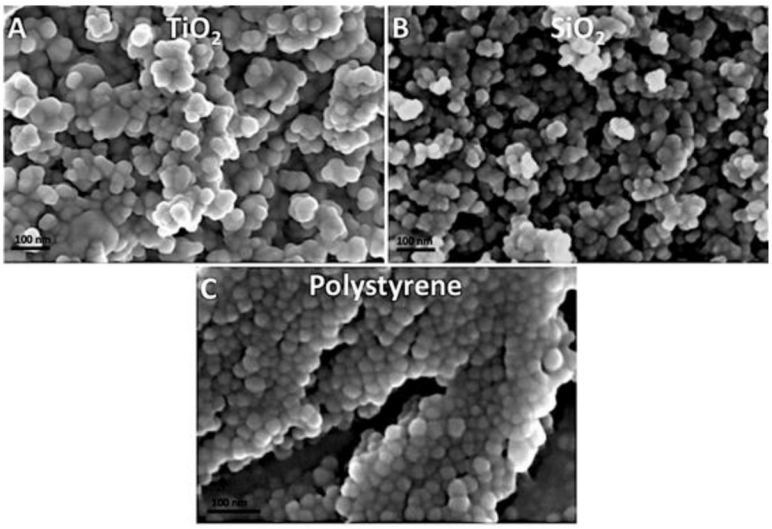

Figure 1.
SEM images of TiO_2, SiO_2, and PS NPs. TiO_2 (A), SiO_2 (B), and PS (C).

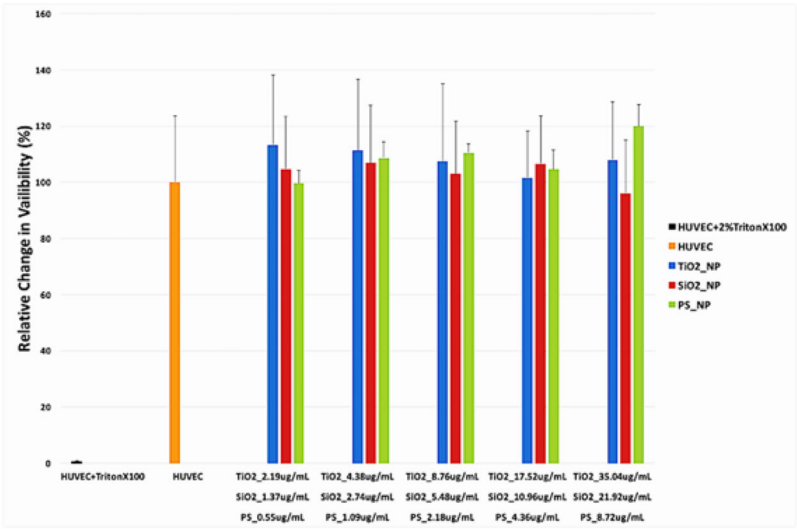

Figure 2.

Viability of HUVEC exposed to TritionX100 (negative control), TiO_2, SiO_2, and PS NPs. HUVEC were exposed in triplicate to surface area-matched concentrations of TiO_2, SiO_2, and PS NPs for 24 hours. Viability was then measured using CCK-8. (Error bars represent mean ± standard deviation (SD) of the sample. Data were analyzed with a one way ANOVA, no results were significantly different from untreated HUVEC, $n = 3$, $p > 0.05$.)

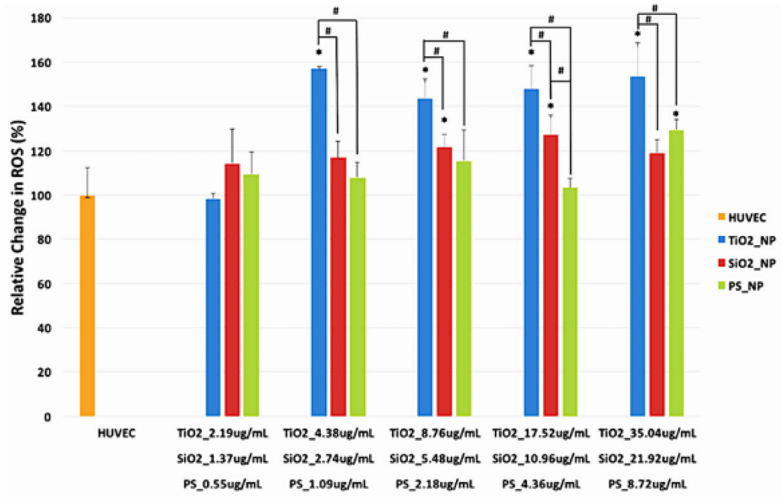

Figure 3.

ROS level in HUVEC exposed to TiO_2, SiO_2, and PS NPs. HUVEC were exposed in quadruplicate to various concentrations of TiO_2, SiO_2, and PS NPs for 24 hours. ROS level was then measured using H2DCFDA. (Error bars represent mean ± standard deviation (SD) of the sample. Data were analyzed by ANOVA with Tukey's post test, * represents significant difference from untreated HUVEC, # denotes significant difference within the group, n=4, $p < 0.05$.)

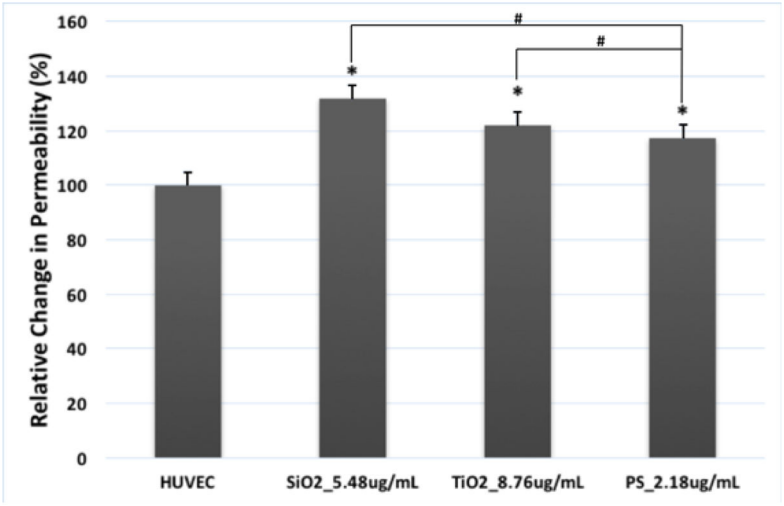

Figure 4.

Exposure to TiO_2, SiO_2 and PS NPs disrupted endothelial barrier function in HUVEC. HUVEC were exposed to TiO_2, SiO_2 and PS NPs at the concentrations that three types of NPs have the same total surface area (8.76 μg/mL or 2.65 μg/cm^2 for TiO_2 NPs, 5.48 μg/mL or 1.66 μg/cm^2 for SiO_2 NPs, 2.18 μg/mL or 0.66 μg/cm^2 for PS NPs). Control was treated with fresh EGM-2. FITC-dextran fluorescence in the bottom chamber was measured after 2 hours of exposure to all three types of NPs. Mean ± standard deviation (SD) of the sample. Data were analyzed by one way ANOVA, * represents significant difference compared with untreated HUVEC, # denotes significant difference between different NPs, $n = 3$, $p < 0.05$.

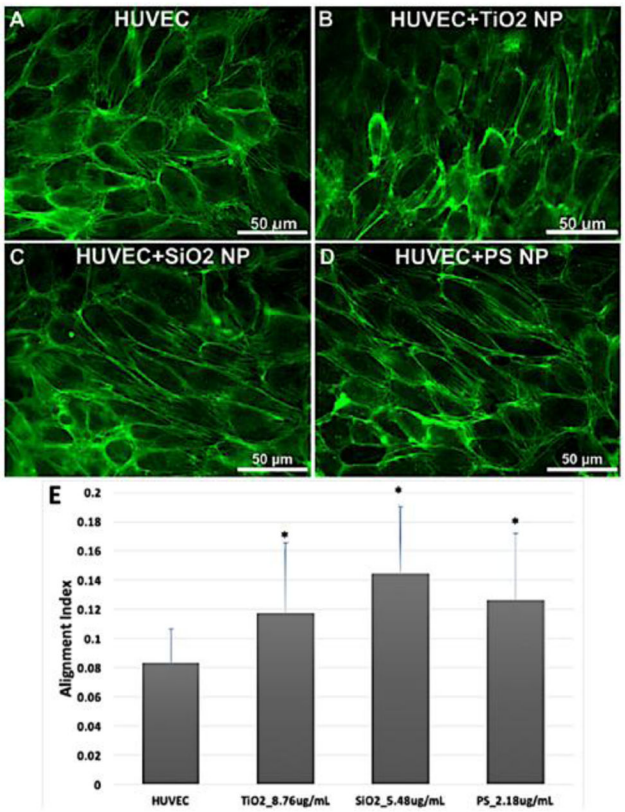

Figure 5.

Actin rearrangement induced by TiO_2, SiO_2 and PS NPs exposure. HUVEC treated with TiO_2, SiO_2 and PS NPs at the concentrations that three types of NPs have the same total surface area (8.76 μg/mL or 2.65 μg/cm^2 for TiO_2 NPs, 5.48 μg/mL or 1.66 μg/cm^2 for SiO_2 NPs, 2.18 μg/mL or 0.66 μg/cm^2 for PS NPs) were fixed and labeled for actin after 2 hours of exposure. Control was treated with fresh EGM-2. Control (A), TiO_2 (B), SiO_2 (C) and PS (D). The actin microfilaments were rearranged and aligned after 2-hour exposure (E). Mean ± standard deviation (SD) of the sample. Data were analyzed by one way ANOVA, * denotes significant difference compared with untreated HUVEC, $n = 15$, $p < 0.05$.

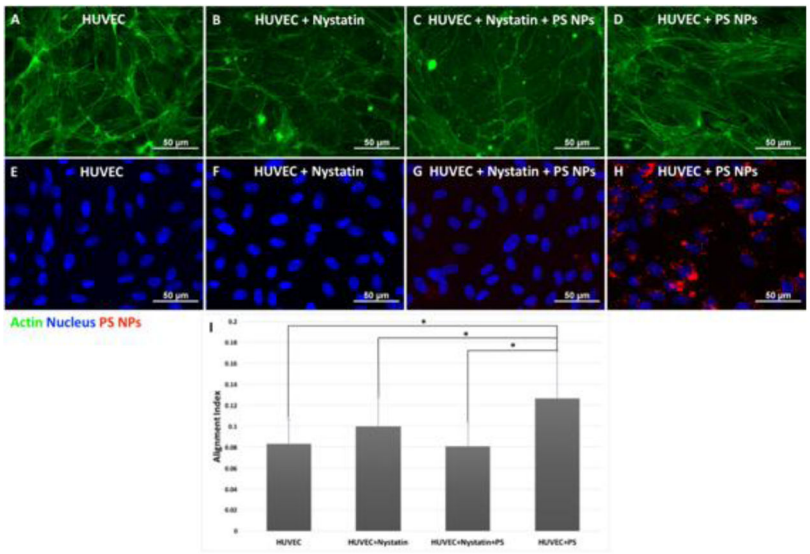

Figure 6.

The inhibition of caveolae/raft-mediated endocytosis prevented actin microfilament alignment. Confluent layer of HUVEC cells were treated with 25 μM caveolae/raft-mediated endocytosis inhibitor, Nystatin for 2 hours prior to 2-hour PS nanoparticle exposure at 2.18 μg/mL or 0.66 μg/cm^2. HUVEC after exposure to 20 nm PS NPs, actin (G), nucleus and PS NPs (H). HUVEC pretreated with Nystatin after exposure to 20 nm PS NPs, actin (E), nucleus and PS NPs (F). The 20 nm PS NPs-induced actin alignment was prevented by inhibiting the caveolae/raft-dependent endocytosis (E). Mean ± standard deviation of the sample. Date were analyzed with one way ANOVA, * denotes significant difference between comparisons, $n = 20$, $p < 0.05$.

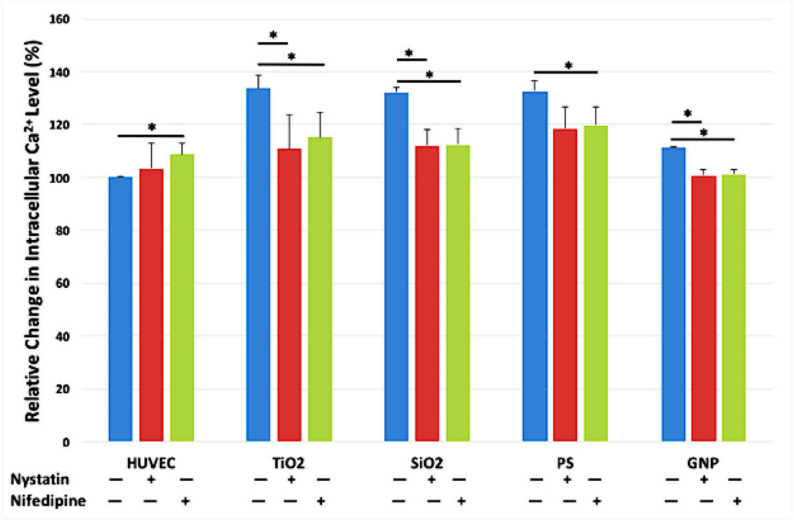

Figure 7.

Intracellular Ca^{2+} Level of HUVEC after nanoparticle exposure was measured using Fura-2 AM. Caveolae/raft-dependent endocytosis was inhibited by pretreating the cells with 25 μM Nystatin for 2 hours, and L-type calcium channel was blocked by pretreating the cells with 10 μM Nifedipine for 2 hours. Then cells were treated with TiO_2, SiO_2, PS NPs, and GNPs at the concentrations that yield the same total surface area (8.76 μg/mL or 2.65 μg/cm^2 for TiO_2 NPs, 5.48 μg/mL or 1.66 μg/cm^2 for SiO_2 NPs, 2.18 μg/mL or 0.66 μg/cm^2 for PS NPs, and 40 μg/mL or 21.96 μg/cm^2 for GNPs) for 2 hours; control was treated with fresh EGM-2. Mean ± standard deviation (SD) of the sample. Data were analyzed by ANOVA with Tukey's post test, * denotes significant difference comparisons, $n = 4$, $p < 0.05$.

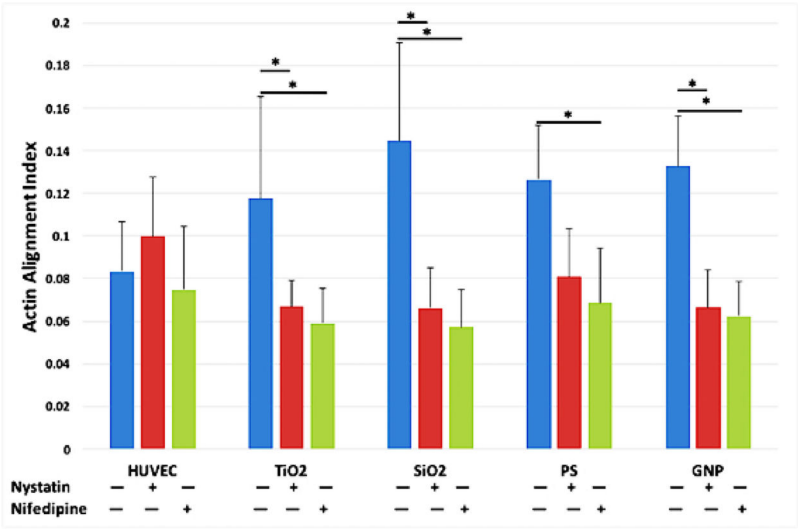

Figure 8.

The inhibition of caveolea/raft-mediated endocytosis and calcium channel prevented actin microfilaments alignment. Caveolae/raft-dependent endocytosis was inhibited by pretreating the cells with 25 μM Nystatin for 2 hours, and L-type calcium channel was blocked by pretreating the cells with 10 μM Nifedipine for 2 hours. Then cells were treated with TiO_2, SiO_2, PS, and GNPs at the concentrations that yield the same total surface area (8.76 μg/mL or 2.65 μg/cm^2 for TiO_2 NPs, 5.48 μg/mL or 1.66 μg/cm^2 for SiO_2 NPs, 2.18 μg/mL or 0.66 μg/cm^2 for PS NPs, and 40 μg/mL or 21.96 μg/cm^2 for gold NPs) for 2 hours; control was treated with fresh EGM-2. Mean ± standard deviation of the sample. Data were analyzed by ANOVA with Tukey's post test, * denotes significant difference between comparisons, n = 20, $p < 0.05$.

Table 1

Hydrodynamic size, polydispersity index, zeta potential and dry size of TiO_2, SiO_2, and PS NPs. NTA, DLS and zeta potential samples were prepared in DI water. Over 50 particles of each type of GNPs were measured from SEM images. Results are presented as mean ± standard deviation (SD).

Nanoparticle	Size (nm) (NTA)	Size (nm) (DLS)	ζ-Potential (mv) (DLS)	Polydispersity Index (PDI) (DLS)	Size (nm) (SEM)
TiO2	103.7±42.2 (DI)	120.6±30.6 (DI)	−44.3 (DI)	0.154 (DI)	31.6±3.0
	140.6±1.1 (EGM-2)	174.8±3.0 (EGM-2)	−9.5 (EGM-2)	0.31 (EGM-2)	
SiO2	121.8±38.3 (DI)	219.9±65.6 (DI)	−46.1 (DI)	0.129 (DI)	26.6±3.8
	204.0±0.5 (EGM-2)	254.5±0.72 (EGM-2)	−7.9 (EGM-2)	0.27 (EGM-2)	
PS	81.1±16.4 (DI)	-	-	-	25.0±2.0
	93.7±2.0 (EGM-2)	-	-	-	